Rethinking the role of transport and photochemistry in regional ozone pollution: Insights from ozone concentration and mass budgets

Kun Qu[1,2,3], Xuesong Wang[1,2], Xuhui Cai[1,2], Yu Yan[1,2], Xipeng Jin[1,2], Mihalis Vrekoussis[3,4,5], Maria Kanakidou[3,6], Guy Brasseur[7,8], Jin Shen[9], Teng Xiao[1,2], Limin Zeng[1,2], and Yuanhang Zhang[1,2,10,11]

[1]State Key Joint Laboratory of Environmental Simulation and Pollution Control, College of Environmental Sciences and Engineering, Peking University, Beijing 100871, China
[2]International Joint Laboratory for Regional Pollution Control, Ministry of Education, Beijing, 100816, China
[3]Laboratory for Modeling and Observation of the Earth System (LAMOS), Institute of Environmental Physics (IUP), University of Bremen, Bremen, Germany
[4]Center of Marine Environmental Sciences (MARUM), University of Bremen, Germany
[5]Climate and Atmosphere Research Center (CARE-C), The Cyprus Institute, Cyprus
[6]Environmental Chemical Processes Laboratory, Department of Chemistry, University of Crete, Heraklion, Greece
[7]Max Planck Institute for Meteorology, Hamburg, Germany
[8]National Center for Atmospheric Research, Boulder, Colorado, USA
[9]State Key Laboratory of Regional Air Quality Monitoring, Guangdong Key Laboratory of Secondary Air Pollution Research, Guangdong Environmental Monitoring Center, Guangzhou 510308, China
[10]Beijing Innovation Center for Engineering Science and Advanced Technology, Peking University, Beijing 100871, China
[11]CAS Center for Excellence in Regional Atmospheric Environment, Chinese Academy of Sciences, Xiamen 361021, China

Correspondence to: Xuesong Wang (xswang@pku.edu.cn) and Yuanhang Zhang (yhzhang@pku.edu.cn)

Abstract. Understanding the role of transport and photochemistry is essential to mitigate tropospheric ozone (O_3) pollution within a region. In previous studies, the O_3 concentration budget has been widely used to determine the contributions of two processes to the variations of O_3 concentrations. These studies often conclude that local photochemistry is the main cause of regional O_3 pollution; however, they fail to explain why O_3 in a targeted region is often primarily derived from O_3 and/or its precursors transported from the outside regions as reported by many studies of O_3 source apportionment. Here, we present a method to calculate the hourly contributions of O_3-related processes to the variations of not only the mean O_3 concentration, but also the total O_3 mass (the corresponding budgets are noted as the O_3 concentration and mass budget, respectively) within the atmospheric boundary layer (ABL) of the concerned region. Based on the modelling results of WRF-CMAQ, the two O_3 budgets were applied to comprehensively understand the effects of transport and photochemistry on the O_3 pollution over the Pearl River Delta (PRD) region in China. Quantified results demonstrate the different role of transport and photochemistry when comparing the two O_3 budgets: Photochemistry drives the rapid increase of O_3 concentrations during the day, whereas transport, especially vertical exchange through the ABL top, controls both rapid O_3 mass increase in the morning and decrease in the afternoon. The diurnal changes of the transport contributions in the two O_3 budgets highlight the influences of the ABL diurnal cycle and regional wind fields on regional O_3 pollution. Through high contributions to the O_3 mass increase in the morning, transport determines that most O_3 in the PRD originates from the global background and emissions outside the region. However, due to the simultaneous rapid increase of ABL volumes, this process only has a relatively limited effect on O_3 concentration increase compared to photochemistry, and transport effect on the regional sources of O_3 cannot be illustrated by

37 the O_3 concentration budget. For future studies targeting O_3 and other secondary pollutants with moderately long atmospheric

38 lifetimes (e.g., fine particulate matter and some of its components), insights from both concentration and mass budgets are

39 required to fully understand the role of transport, chemistry and other related processes.

1 Introduction

41 Since first recognized as a key contributor to the Los Angeles smog, tropospheric ozone (O_3) pollution has received

42 considerable attention in many highly populated areas in the world (Fishman et al., 2003; Schultz et al., 2017; Fleming et al.,

43 2018; Fowler et al., 2020). Exposure to O_3 threatens crop yields, ecosystems and human health, resulting in increased

44 mortality and economic losses (Mills et al., 2013; Ainsworth, 2017; Zhang et al., 2019). In addition, O_3 contributes to global

45 warming not only directly as a greenhouse gas, but also indirectly by damaging plants and suppressing land carbon sinks

46 (Sitch et al., 2007; Naik et al., 2021). To address these detrimental effects, efforts have been undertaken to reduce O_3 levels

47 in polluted regions. However, since O_3 is a secondary pollutant produced in the atmosphere by complex non-linear

48 chemistry, the abatement of O_3 pollution is a challenging task.

49

50 As a prerequisite to effectively control O_3 pollution, firstly, it is imperative to understand the effects of O_3-related processes

51 on the abundance of O_3 in the atmosphere. High O_3 concentrations within a region are often attributed to daytime

52 photochemical production from O_3 precursors, i.e. NO_x (= NO + NO_2) and volatile organic compounds (VOCs), under

53 sunlight. Due to the short lifetime of O_3 precursors (several hours for NO_x and reactive VOCs (Liu et al., 2016; Seinfeld and

54 Pandis, 2016; Laughner and Cohen, 2019)), it is generally believed that O_3 photochemistry is mainly linked to the

55 contributions of local emissions in polluted regions. On the other hand, since O_3 itself has a moderately long atmospheric

56 lifetime of 20-30 days (Stevenson et al., 2006; Bates and Jacob, 2019), transport processes in the atmosphere, including

57 horizontal transport (mainly advection) and vertical exchange through the top of the atmospheric boundary layer (ABL), may

58 also considerably contribute to regional O_3 pollution (Myriokefalitakis et al., 2016). Specifically, through vertical exchange,

59 O_3 in the residual layer and/or free atmosphere is entrained into the ABL and involved in the ABL mixing after sunrise,

60 leading to rapidly increasing O_3 concentrations near the surface (Kaser et al., 2017; Hu et al., 2018; Zhao et al., 2019).

61 Although O_3 produced from local emissions may be transported out and later recirculated back to the region, it is more likely

62 that transported O_3 is mainly derived from the emissions of O_3 precursors in the upwind regions, continents and even O_3 in

63 the stratosphere under the combined effect of meso-, synoptic-, large- and global-scale atmospheric movements (Massagué

64 et al., 2019). If photochemistry has a comparatively large influence on O_3, reducing local emissions is an appropriate strategy

65 to alleviate regional O_3 pollution; otherwise, it is necessary to focus on emission control in the upwind regions, aiming to

66 reduce transport contributions to O_3.

67

68   In many studies, the O_3 concentration budget was often utilized to quantify the contributions of various transport and

69   chemical processes to the variations of O_3 concentrations. The changes in the mean O_3 concentration within the ABL ($\langle c_{O_3} \rangle$)

70   can be expressed as the net contributions of all O_3-related processes (Lenschow et al., 1981; Janssen and Pozzer, 2015; Vilà-

71   Guerau de Arellano et al., 2015):

$$\frac{\partial \langle c_{O_3} \rangle}{\partial t} = -\bar{u}\frac{\partial \langle c_{O_3} \rangle}{\partial x} - \bar{v}\frac{\partial \langle c_{O_3} \rangle}{\partial y} - \frac{\partial \overline{c_{O_3}'w'}}{\partial z} + S(O_3) \tag{1}$$

72   where u, v and w refer to wind speeds in the x-, y- and z-direction, respectively. The right side of Eq. (1) describes the

73   contributions of 1) horizontal transport (advection, the first two terms), 2) vertical exchange through the ABL top

74   (entrainment and detrainment, the third term), 3) gas-phase chemistry, dry deposition and other processes (the term $S(O_3)$

75   indicates their net contributions). The O_3 concentration budget is then derived by integrating these terms over time. It enables

76   the identification of the processes that produce positive or negative tendencies of the O_3 concentration, and of the processes

77   that are most influential for regional O_3 pollution. Reported O_3 concentration budgets derived from ground-based

78   measurements (Su et al., 2018; Tan et al., 2018; Tan et al., 2019; Yu et al., 2020), aircraft-based mobile observations

79   (Lenschow et al., 1981; Trousdell et al., 2016; Trousdell et al., 2019) and Process Analysis (PA) or similar modules in

80   chemical transport models (Hou et al., 2014; Li et al., 2021; Yan et al., 2021) in various regions of the globe often suggest

81   that O_3 production through local photochemistry drives the noon-time increase of O_3 concentration, whereas transport

82   reduces O_3 concentration over the same period. Conclusively, photochemistry, rather than transport, plays a main role in O_3

83   pollution.

84

85   However, O_3 source apportionment is likely to provide different conclusions about the relative importance of transport and

86   photochemistry in affecting O_3 pollution. O_3 source apportionment is performed to identify the regional and/or sectoral

87   origins of O_3, of which the results are also used to support air pollution control (Clappier et al., 2017; Thunis et al., 2019).

88   Here, we only discuss the regional origins of O_3, because the contributions of sources outside the region (or emissions within

89   the region, defined as local emissions hereafter) provide information on the influence of transport (or photochemistry) on O_3

90   pollution. Previous publications often conclude that most O_3 was not derived from local emissions of O_3 precursors, but from

91   the global background and emissions outside the targeted regions (Guo et al., 2018; Pay et al., 2019; Liu et al., 2020). The

92   mixing ratios of background O_3 in various regions of the world are mostly within the range of 30-50 ppb (Reid et al., 2008

93   and references therein), which are sufficiently high to ensure that O_3 originates mainly from non-local sources in less

94   polluted regions. Since controlling background O_3 is challenging, efforts to control O_3 pollution in polluted regions with high

95   non-local contributions to O_3 should focus on reducing emissions in upwind regions rather than only local areas (Lelieveld et

96   al., 2009; Boian and Andrade, 2012; Massagué et al., 2019). One successful example is the establishment of the "Ozone

97   Transport Region" in the north-eastern United State by the US Environmental Protection Agency, which promotes

98   collaborative emission reductions among states to address inter-state O_3 transport (Novel, 1992). The above discussion

99   highlights the importance of transport for regional O_3 pollution, since it often plays a more prominent role than local

100   photochemistry. Apparently, this last statement conflicts with the conclusions derived from the O_3 concentration budget.

101   Thus, while the O_3 concentration budget is useful for understanding O_3 pollution, it may not completely illustrate the effects

102   of transport and photochemistry on regional O_3 pollution.

103

104   In the ABL of the concerned region, the mean O_3 concentration and total O_3 mass are both conserved, which means that their

105   variations are equal to the net contributions by various O_3-related processes including transport and photochemistry. These

106   relationships can be represented by the O_3 concentration budget and mass budget, respectively. Unlike the aforementioned

107   O_3 concentration budget in Eq. (1), the hourly O_3 mass budget, written as

$$\frac{\partial m_{O_3}}{\partial t} = -\left(\bar{u}s_x\langle c_{O_3}\rangle + \bar{v}s_y\langle c_{O_3}\rangle\right) - \overline{c_{O_3}'w'}s_z + S(O_3)V \tag{2}$$

108   is seldom reported (m_{O_3} is the total O_3 mass within the ABL of the region; s_x, s_y, s_z are the areas of the interfaces in the x-,

109   y- and z-direction, respectively; V is the volume of the ABL column). Due to the varied effects of transport on O_3

110   concentration and mass, the O_3 mass budget differs from the O_3 concentration budget but is more suitable to explore the

111   influence of transport and photochemistry on the results of O_3 source apportionment (more detailed explanations are given in

112   Sect. 2.4). In order to comprehensively understand the role of transport and photochemistry in regional O_3 pollution, in the

113   present study, we developed a method to calculate both the O_3 concentration and mass budget based on the simulation results

114   from the Weather Research and Forecasting (WRF) and Community Multiscale Air Quality (CMAQ) models, and also

115   analysed, compared the results of the two regional-level O_3 budgets. The Pearl River Delta (PRD) region, a city cluster

116   located on the southeast coast of China and exposed to severe O_3 pollution in summer and autumn (Gao et al., 2018), was

117   selected as the targeted region. The tasks for this study can be summarized as follows:

118

119   *1) Development of the method to quantify the two O_3 budgets*

120   WRF-CMAQ employs the Process Analysis (PA) module to assess the contributions of O_3-related processes to the variations

121   of O_3 concentrations within each grid cell. However, to obtain the regional-level O_3 concentration and mass budgets, the

122   results of PA module are not sufficient. One reason is that the contribution of vertical exchange through the ABL top is not

123   specifically quantified in commonly used ABL parameterizations, thus requires additional calculations (Kaser et al., 2017).

124   Additionally, calculations based on the PA results are needed to identify the contributions of other O_3-related processes to

125   ABL-mean O_3 concentration as well as the results of the O_3 mass budget. To address this, we developed a method to quantify

126   the two O_3 budgets, of which the details are given in Sect. 2.1-2.3.

127

128   *2) Analysis and comparison of the results from the two O_3 budgets*

129   Based on the simulations of O_3 pollution in the PRD with the model setup introduced in Sect. 2.5, the two O_3 budgets were

130   calculated for further analyses and comparisons to reveal the role of transport and photochemistry in regional O_3 pollution

131   from a more comprehensive perspective. Relative discussions are presented in Sect. 3.

132

3) Assessment of the role of transport and photochemistry in determining the regional origins of O₃

The Brute Force Method (BFM; Clappier et al., 2017), a widely used source apportionment method, was combined with the O₃ mass budget calculation to determine the contributions of emissions within and outside the PRD as well as background sources to the O₃ transported into or produced by photochemistry in the region (methodology described in Sect. 2.6). The results, as discussed in Sect. 4, reveal the impacts of transport and photochemistry in determining the regional origins of O₃ in the PRD, and explain why the different views on the role of two processes in regional O₃ pollution are suggested by the O₃ concentration budget and O₃ source apportionment studies.

2 Methodology: O₃ budget calculations and model setup

2.1 The PRD grids and O₃-related processes in O₃ budgets

The two O₃ budgets were calculated for the PRD, of which the grids are shown in the lower-left panel of Fig. 1. These grids are set based on the finer modelling domain of WRF-CMAQ (details given in Sect. 2.5) and determined according to the administrative areas of the PRD. The PRD grids with one or several interfaces with the outer regions are defined as the border grids, and they can be further classified as the grids in the north, south, west and east borders based on their locations. Correspondingly, the PRD grids with no interface with the outer regions are defined as the non-border grids.

Figure 1 also displays all O₃-related processes considered in the calculation of O₃ budgets here. The transport processes include horizontal transport through the four types of borders and vertical exchange through the ABL top. For vertical exchange, its contribution in the O₃ concentration budget (the third term on the right side of Eq. (1)) is quantified by (Sinclair et al., 2010; Jin et al., 2021):

$$-\frac{\partial \overline{c_{O_3}'w'}}{\partial z} = \frac{\Delta c_{O_3}}{H}\frac{\partial H}{\partial t} + \frac{\Delta c_{O_3}}{H}\left(u_h\frac{\partial H}{\partial x} + v_h\frac{\partial H}{\partial y} - w_h\right) \tag{3}$$

where H is the ABL height; Δc_{O_3} is the difference between O₃ concentrations above and within the ABL; u_h, v_h and w_h are the ABL-top wind speeds in the x, y and z-direction, respectively. The terms on the right side of Eq. (3) suggest that vertical exchange through the ABL top, or entrainment and detrainment, is attributed to 1) the temporal changes of ABL heights (H) and 2) advection perpendicular to the ABL top and its slope. For the convenience of discussion, hereafter, vertical exchanges due to the above two dynamic processes are marked as ABLex-H and ABLex-A, respectively. The contributions of all transport processes in the O₃ budgets were quantified based on meteorological parameters simulated by WRF and O₃ concentrations simulated by CMAQ. The basic calculations of the contributions from the above-mentioned transport processes in the O₃ mass and concentration budgets are separately introduced in the following two sections.

160

5
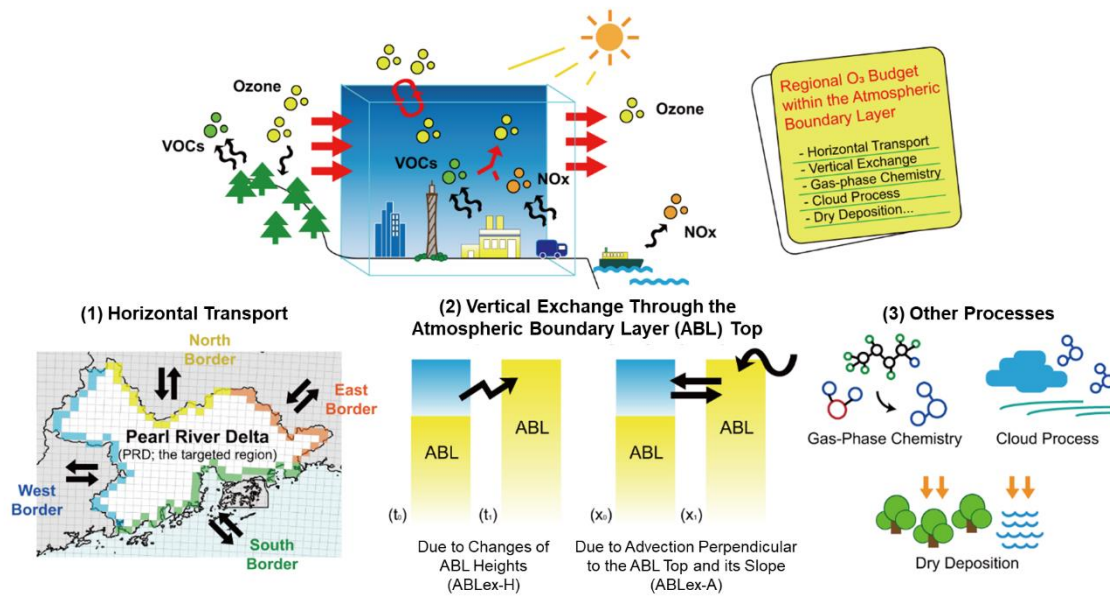
Figure 1. Schematic illustration of O_3 budgets (the upper panel) and O_3-related processes considered (the lower panel): (1) Horizontal transport through the north, south, west and east borders of the Pearl River Delta (PRD) (the distributions of the PRD grids are also shown: yellow, green, blue, orange for the north, south, west and east border grids, respectively, and white for the non-border grids); (2) Vertical exchange through the atmospheric boundary layer (ABL) top, including the process due to the changes of ABL heights (ABLex-H) and advection perpendicular to the ABL top and its slope (ABLex-A); (3) Other processes, including gas-phase chemistry, cloud process and dry deposition for this study.

Other processes in the O_3 budgets include gas-phase chemistry (including daytime photochemical O_3 production, O_3 titration by NO and O_3 depletion with unsaturated VOCs, etc.), cloud process (including below and in-cloud mixing, aqueous-phase chemistry, wet deposition; Liu et al., 2011) and dry deposition. The contributions of these processes are all calculated based on the output of the PA module in CMAQ. In a word, their contributions in the O_3 mass budget are obtained by summing up the contributions in all grid cells within the ABL of the PRD, and their contributions in the O_3 concentration budget are the corresponding contributions to O_3 mass divided by the volume of the ABL of the PRD. Since diffusion through the side and top boundaries of the region is expected to have a negligible influence on the variations of both O_3 concentration and mass, we did not consider this process in O_3 budget calculations.

The calculation process of the two O_3 budgets is summarized as follows. Based on multiple output files of WRF and CMAQ, firstly, the contributions of all considered O_3-related processes to O_3 mass changes and volumes/volume changes linked to these processes within the ABL are calculated in nearly all grids of the modelling domain. We developed the post-processing tool *flux_4d_cal* to conduct the above calculations. Afterwards, the regional-level O_3 mass and concentration budgets are quantified based on the results of the first-step calculations. Particularly, the method described in Sect. 2.3 is applied to

183   estimate the contributions of O_3-related processes in the O_3 concentration budget. More detailed descriptions of the

184   calculation process can be found in Text S1.

2.2 Transport contributions in the O_3 mass budget

186   The method by Yang et al. (2012) and Chang et al. (2018) was applied to quantify the contributions of horizontal transport in

187   the O_3 mass budget. For instance, the contribution of the advection through the west/east interface of a grid column within

188   the ABL to total O_3 mass (F_{htrans}) in the column during the time interval dt is calculated as:

$$F_{htrans} = \int_0^H c_{O_3} u L \, dz \, dt \tag{4}$$

189   where L is the width of the grid (equal to the horizontal resolution in the model); dz is the height of vertical layers. For

190   advection through the north/south interface, the calculation is similar to Eq. (4), except for using v instead of u. F_{htrans}

191   values through all interfaces between the border grids and the outer region were calculated. Afterwards, they are summed up

192   separately according to the types of borders as the net contributions of horizontal transport through the north, south, west and

193   east borders of the PRD in the O_3 mass budget.

194

195   Following Sinclair et al. (2010) and Jin et al. (2021), the contribution of vertical exchange through the ABL top to O_3 mass

196   (F_{ABLex}) during the time interval dt can be expressed as:

$$F_{ABLex} = F_{ABLex-H} + F_{ABLex-A} = c_{O_{3\_h}} \frac{\partial H}{\partial t} L^2 dt + c_{O_{3\_h}} \left(u_h \frac{\partial H}{\partial x} + v_h \frac{\partial H}{\partial y} - w_h \right) L^2 dt \tag{5}$$

197   where $c_{O_{3\_h}}$ is the O_3 concentration at the ABL top. The two terms on the right-most side of Eq. (5) separately describe the

198   contributions of ABLex-H and ABLex-A (separately denoted as $F_{ABLex-H}$ and $F_{ABLex-A}$). F_{ABLex} values in all the grids over

199   the PRD were summed up to derive the net contribution of vertical exchange through the ABL top in the O_3 mass budget.

2.3 Transport contributions in the O_3 concentration budget

201   It is difficult to directly apply Eq. (1) in the quantification of transport contributions in the regional-level O_3 concentration

202   budget. Therefore, a different approach was applied, which is introduced as follows.

203

204   Suppose that an air parcel with a total volume of dV is transported into the ABL of the PRD (its original volume is V). The

205   variation of $\langle c_{O_3} \rangle$ under the influence of horizontal transport ($d\langle c_{O_3} \rangle_{htrans}$) can be written as:

$$d\langle c_{O_3} \rangle_{htrans} = \frac{F_{htrans} + \langle c_{O_3} \rangle (V - dV)}{V} - \langle c_{O_3} \rangle = \frac{F_{htrans} - \langle c_{O_3} \rangle \, dV}{V} \tag{6}$$

206   Since ABLex-A is also an advection process, its contribution in the O_3 concentration budget ($d\langle c_{O_3} \rangle_{ABLex-A}$) can be

207   quantified using a similar formula as Eq. (6), except for using $F_{ABLex-A}$ instead of F_{htrans}.

208

209 Through ABLex-H, air parcels in the residual layer and/or free atmosphere are merged into the ABL or vice versa. Thus, the
210 variation of $\langle c_{O_3} \rangle$ under its influence ($d\langle c_{O_3} \rangle_{ABLex-H}$) is expressed as:

$$d\langle c_{O_3} \rangle_{ABLex-H} = \frac{F_{ABLex-H} + \langle c_{O_3} \rangle V}{V + dV} - \langle c_{O_3} \rangle = \frac{F_{ABLex-H} - \langle c_{O_3} \rangle \, dV}{V + dV} \tag{7}$$

211

212 If the targeted region is small enough, the expressions of $d\langle c_{O_3} \rangle_{htrans}$ and $d\langle c_{O_3} \rangle_{ABLex-H}$ in Eqs. (6) and (7) can be
213 transformed to the corresponding terms in Eq. (1), confirming the applicability of the above calculations (for details, see
214 Text S2). All variables in Eqs. (6) and (7) can be quantified by the post-processing tool *flux_4d_cal*, making the method
215 feasible and suitable for the afterward calculations of the regional-scale O_3 concentration budget.

216

217 However, due to the prominent diurnal cycle of ABL, V in Eqs. (6) and (7) may change notably within an hour, leading to
218 bias in the hourly estimations of $d\langle c_{O_3} \rangle_{htrans}$, $d\langle c_{O_3} \rangle_{ABLex-H}$ and $d\langle c_{O_3} \rangle_{ABLex-A}$ when using V at the start and end of the
219 hour. This problem also applies to the calculation of contributions from other O_3-related processes. In order to reduce the
220 potential bias caused by the different selections of V, we designed two calculation paths for the hourly O_3 concentration
221 budget (Fig. S1):

222 • O_3 mass change → ABL volume change
223 • ABL volume change → O_3 mass change

224 where only O_3 mass or ABL volume changes in each calculation step. The contribution of ABLex-H to O_3 concentration can
225 be viewed as the net effects of ABL volume change and O_3 being transported into/out of the ABL: ABL volume change due
226 to ABL development (collapse) leads to lower (higher) O_3 concentration, and O_3 transported into (out of) the ABL through
227 ABLex-H leads to O_3 increase (decrease). These contributions are quantified separately in the ABL volume and O_3 mass
228 change steps. The contributions of horizontal transport, ABLex-A and non-transport processes are quantified only in the O_3
229 mass change step. The contribution of each process to the variation of O_3 concentration is calculated using both paths, and
230 the mean value of two results serves as an estimation close to its real contribution in the O_3 concentration budget.

231 **2.4 Difference between the two O_3 budgets**

232 The difference between the two O_3 budgets is linked to the varied effect of transport on O_3 mass and concentration. Suppose
233 that the mean O_3 concentration in the transported air parcels is $\langle c_{O_3} \rangle_{trans}$. For horizontal transport, its contributions in the O_3
234 mass and concentration budgets can be separately written as:

$$F_{htrans} = \langle c_{O_3} \rangle_{trans} \, dV \tag{8}$$

$$d\langle c_{O_3} \rangle_{htrans} = \frac{dV}{V} \left(\langle c_{O_3} \rangle_{trans} - \langle c_{O_3} \rangle \right) \tag{9}$$

235 Apparently, F_{htrans} is related to the O_3 concentrations in the transported air parcels, but not to those in the studied region. It
236 indicates the amount of O_3 mass transported into or out of the region. Whether it is positive or negative only depends on the

8

237   direction of transport — O₃ being transported into (out of) the region leads to the increase (decrease) of O₃ mass, which

238   corresponds to a positive (negative) contribution in the O₃ mass budget. In contrast, $d\langle c_{O_3}\rangle_{htrans}$ quantifies how much

239   horizontal transport alters regional-mean O₃ concentrations, and is linked to the difference between O₃ concentrations in the

240   transported air parcels and the studied region (Eq. (9)). O₃ being transported into (out of) the region does not necessarily

241   result in a higher (lower) O₃ concentration. For instance, when clean air parcels with relatively low O₃ levels ($\langle c_{O_3}\rangle_{trans} <$

242   $\langle c_{O_3}\rangle$) are transported into the region, they dilute O₃ pollution and reduce O₃ concentration ($d\langle c_{O_3}\rangle_{htrans} < 0$). Given that

243   ABLex-A is also an advection process, the above difference also applies to it. For ABLex-H, its contributions in the O₃ mass

244   and concentration budgets are expressed as:

$$F_{ABLex-H} = \langle c_{O_3}\rangle_{trans} \, dV \qquad (10)$$

$$d\langle c_{O_3}\rangle_{ABLex-H} = \frac{dV}{V + dV}\left(\langle c_{O_3}\rangle_{trans} - \langle c_{O_3}\rangle\right) \qquad (11)$$

245   Similarly, ABL development and collapse lead to the increase and decrease of O₃ mass, respectively, but whether they

246   contribute to higher or lower O₃ concentration also depends on the difference between O₃ concentration in the transported air

247   parcels and that in the region. Based on the above discussion, these transport processes all show different effects on O₃ mass

248   and concentration — the effect of transport on the variations of O₃ mass is only related to the characteristics of the

249   transported air parcels, namely their volumes and O₃ concentrations within (Eqs. (8) and (10)), while how transport

250   contributes to the variations of O₃ concentration is linked to the difference between O₃ concentrations in the transported air

251   parcels and the region (Eqs. (9) and (11)).

252

253   To properly analyse the impact of transport and photochemistry on the regional origins of O₃, it is required to identify the

254   regional origins of the "new O₃" into the studied region and the "disappeared O₃" out of the studied region contributed by

255   various O₃-related processes, rather than how these processes lead to the variations of O₃ concentration. Thus, the influence

256   of transport and photochemistry on the results of O₃ source apportionment can be explored by the O₃ mass budget, but not by

257   the O₃ concentration budget. By utilizing the BFM source apportionment method in combination with the O₃ mass budget

258   calculation, we can identify the regional origins of O₃ mass increase and decrease due to transport and photochemistry, and

259   explain how these processes determine the results of O₃ source apportionment in the PRD.

260   **2.5 Model setup and validation**

261   The O₃ concentration and mass budgets within the ABL of the PRD were calculated based on the WRF-CMAQ modelling

262   results by Qu et al. (2021a). The WRF (version 3.2) and CMAQ (version 5.0.2) models were used to simulate the

263   meteorological and pollutant fields, respectively. Two domains with the resolution of 36 and 12 km (denoted as d01 and d02

264   hereafter) were set up for the one-way nested simulations, and the results in the finer d02, which includes the PRD and most

265   areas in East and Central China (Fig. 2), were used in the calculations of O₃ budgets. To represent the contributions of global

266   background to O₃, the initial and boundary conditions for the coarse d01 domain were provided from the global model, the

267   Model for Ozone and Related Chemical Tracers, version 4 (MOZART-4). The PRD inventory provided by the Guangdong

268   Environmental Monitoring Centre, the Multi-resolution Emission Inventory for China (MEIC) inventory for the mainland

269   China (He, 2012), the MIX inventory for the Asian regions outside of mainland China (Li et al., 2017) and biogenic

270   emissions simulated by the Model of Emissions of Gases and Aerosols from Nature (MEGAN; version 2.10) model were

271   used in the simulations. SAPRC07 (Carter, 2010) and AERO6 were applied as the gas-phase chemistry mechanism and the

272   aerosol scheme, respectively. The simulations of O_3 pollution in the PRD were performed for October 2015 (October 11–

273   November 10, 2015) and July 2016 (July 1–31, 2016), which serve as the representative months in autumn and summer,

274   respectively. Here, O_3 polluted days are defined when the maximum hourly O_3 concentrations of the day exceed 200 $\mu g/m^3$,

275   or the maximum 8-hour average O_3 concentrations of the day exceed 160 $\mu g/m^3$ (both are the Grade-II O_3 thresholds in the

276   Chinese National Ambient Air Quality Standard) in any municipality of the PRD. According to this definition, there were 16

277   and 12 O_3 polluted days in the two months, respectively (more information is given in Table S1). The mean O_3 budgets

278   during these O_3 polluted days of two seasons were separately calculated and discussed in the present study.

279
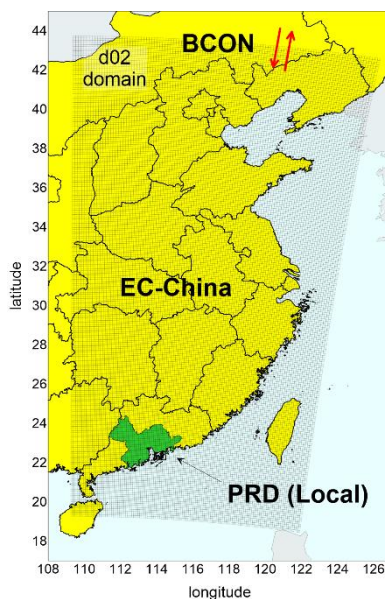
281 **Figure 2.** The spatial distributions of the d02 modelling domain and source regions. The d02 domain is displayed as the nested areas in the
282 figure. PRD, Pearl River Delta; EC-China, East and Central China; BCON, the boundary conditions of d02 modelling, or the contributions
283 of sources outside the d02 domain.

284

285   We evaluated the performance of WRF-CMAQ modelling based on multiple observational datasets. The modelling results of

286   meteorological parameters (including temperature, relative humidity and wind speed), O_3, NO_2 concentrations and the

287   mixing ratios of hydrocarbons have been validated with corresponding observations in the PRD by Qu et al. (2021a). The

288   performance of the model in simulating the above variables was overall satisfying with low biases and high correlations (for

289   details, see Qu et al., 2021a). In this study, we further compared the modelled ABL height, the vertical profiles of wind

290 speed, direction and O_3 mixing ratio in Hong Kong (located in the south PRD) with corresponding observations from the

291 IAGOS (In-service Aircraft for a Global Observing System; Petzold et al., 2015) dataset. The modelled ABL heights showed

292 similar hourly variations during the day as the observational results (R = 0.76), with a mean bias of -1.1 m (Fig. S2). The

293 mean biases of wind speeds are within the range of ± 1 m/s in all considered height ranges (0-1 km, 1-2 km, 2-5 km), and the

294 results of the IAGOS and WRF model indicate similar variations of prevailing wind directions in different seasons and

295 height ranges (Fig. S3). Moreover, modelled O_3 mixing ratios in Oct. 2015 are overestimated by 6% and 26% in the height

296 range of 0-1 km and 1-2 km, respectively, and sufficiently illustrate the development, maintenance and dissipation of O_3

297 pollution during the month (Fig. S4). More detailed evaluations on the model performance of these parameters are presented

298 in Text S3 of the Supplement. Overall, the model performance is acceptable, indicating that the model can provide

299 reasonable data for the calculations of O_3 budgets.

300

301 If the calculation methods and assumptions are reasonable, the conservation of O_3 concentration and mass budgets, described

302 as

$$\frac{\partial \langle c_{O_3} \rangle (or\ m_{O_3})}{\partial t} - \left(S_{htrans} + S_{ABLex} + S_{chem} + S_{cloud} + S_{ddep} \right) = 0 \qquad (12)$$

303 can be achieved (the terms S_{htrans}, S_{ABLex}, S_{chem}, S_{cloud} and S_{ddep} indicate the contributions of horizontal transport, vertical

304 exchange through the ABL top, gas-phase chemistry, cloud process and dry deposition, respectively, in the O_3 concentration

305 or mass budgets). Therefore, we used Eq. (12) to examine the validity of O_3 budget calculations. Total O_3 masses at the start

306 and end of each hour in model output were directly used to calculate the hourly variations of O_3 mass ($\frac{\partial m_{O_3}}{\partial t}$). Besides these

307 two parameters, the volumes of the ABL of the PRD at the start and end of each corresponding hour (calculated using ABL

308 heights in all the PRD grids) are also needed to calculate the hourly variations of O_3 concentration ($\frac{\partial \langle c_{O_3} \rangle}{\partial t}$). The contributions

309 of various O_3-related processes in the O_3 concentration and mass budgets were quantified using the method introduced in

310 Sect. 2.1-2.3. As displayed in Fig. 3, hourly variations of O_3 concentration/mass and the corresponding net contributions

311 from all O_3-related processes show good correlations ($R^2 > 0.9$), with all fitted lines close to the 1:1 line. Thus, the

312 conservation is overall met for the two O_3 budgets in both representative months, allowing for further analyses based on the

313 quantified budgets.

314 **2.6 Identifying regional origins of O_3 mass changes due to transport and photochemistry**

315 The question to be addressed is how O_3-related processes determine the regional origins of O_3. By combining the O_3 mass

316 budget calculations with the BFM source apportionment method, we identified the regional origins of O_3 mass changes due

317 to transport and photochemistry (gas-phase chemistry). Here, the interest lies in the contributions of emissions in the PRD

318 (also defined as local emissions), in other regions within the d02 (mainly East and Central China, hereafter denoted as EC-

319 China), and in regions outside the d02 (the boundary conditions (BCON) of d02 modelling; representative of the background

11

320 sources). The distribution of these source regions is displayed in Fig. 2. Besides the base scenario where all emissions in the

321 d02 were considered in simulations, three sensitivity scenarios were additionally simulated:

- 322 • The PRD_zero scenario: All emissions (including anthropogenic and biogenic emissions; the same below) in the
- 323   PRD are zeroed out;
- 324 • The EC-China_zero scenario: All emissions in the EC-China are zeroed out;
- 325 • The all_zero scenario: All emissions within the d02 are shut down.

326

327
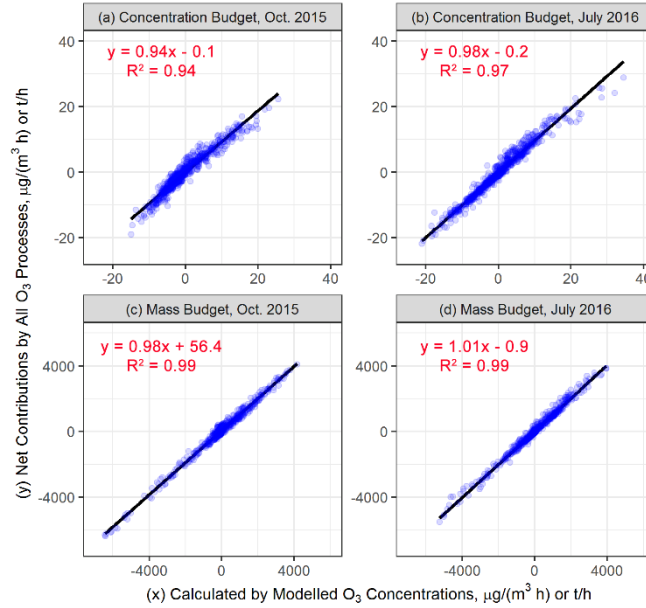
Figure 3. The examinations of O_3 budget conservation in Oct. 2015 (a,c) and July 2016 (b,d) for the hourly O_3 concentration budget (a-b)
and mass budget (c-d). The units for the O_3 concentration and mass budgets are $\mu g/(m^3 \, h)$ and t/h, respectively. The solid black lines in the
plots are the fitted lines.

331 The hourly contributions of the process i in the O_3 mass budget were quantified using the same method outlined in Sect. 2.1-

332 2.2 for the base scenario and three sensitivity scenarios, denoted as $f_{i,base}$, f_{i,PRD_zero}, $f_{i,EC-China\_zero}$, and f_{i,all_zero},

333 respectively. These parameters enable the determination of the contributions of emissions from the PRD and EC-China as

334 well as the background sources (BCON) to the O_3 mass increase and decrease due to various O_3-related processes. The

335 contributions of BCON in the O_3 mass changes due to the process i ($F_{i,BCON}$) can be estimated directly as the contributions of

336 the process i to the O_3 mass in the all_zero scenario:

$$F_{i,BCON} = f_{i,all\_zero} \tag{13}$$

337 For the contributions of the PRD and EC-China emissions from the process i (separately denoted as $F_{i,PRD}$ and $F_{i,EC-China}$),

338 they can be derived in two ways: 1) by subtracting simulations with zeroed studied emissions from the base case simulation

339 (top-down BFM); 2) by subtracting simulations without all emissions from simulations accounting only for studied

12

emissions (bottom-up BFM). Due to the non-linear response of O_3 to precursor emissions, the results from top-down and bottom-up BFM can notably differ, which leads to the non-additivity of the results (the sum of all contributions is not equal to the concerned metric; here, $F_{i,PRD} + F_{i,EC-China} + F_{i,BCON} \neq f_{i,base}$). Therefore, we estimated $F_{i,PRD}$ and $F_{i,EC-China}$ as the average values of the contributions by using top-down BFM and bottom-up BFM:

$$F_{i,PRD} = \frac{1}{2}[(f_{i,base} - f_{i,PRD\_zero}) + (f_{i,EC-China\_zero} - f_{i,all\_zero})] \tag{14}$$

$$F_{i,EC-China} = \frac{1}{2}[(f_{i,base} - f_{i,EC-China\_zero}) + (f_{i,PRD\_zero} - f_{i,all\_zero})] \tag{15}$$

It should be noted that to identify the origins of both "new O_3" into the region and "disappeared O_3" out of the region, the positive and negative contributions of O_3-related processes to the O_3 mass in the PRD grids were separately summed up for the base and sensitivity scenarios and quantified using Eqs. (13-15).

3 Analyses and comparisons of O_3 concentration and mass budget

3.1 O_3 concentration budget

The upper panels of Fig. 4 show the mean diurnal changes of the O_3 concentration budget within the ABL of the PRD. According to the net contributions from all O_3-related processes considered, ABL-mean O_3 concentration increased during most hours in the daytime, with the highest rates occurring in the early morning (8:00-10:00 local time (LT) in autumn, 7:00-9:00 LT in summer). The reduction of ABL-mean O_3 concentration in the late afternoon and at night was also considerable. Its rate reached the maximum value near the sunset time (~18:00 LT in autumn, ~19:00 LT in summer) and gradually decreased throughout the night. The following question is then raised on the suitability of the budget targeting on ABL-mean O_3 concentration to explain the variations of O_3 concentrations near the ground. To answer this question, we compared the hourly changes of modelled ABL-mean O_3 concentration with those of observed and modelled mean near-surface O_3 concentrations in 18 sites of the Guangdong-Hong Kong-Macao PRD Regional Air Quality Monitoring Network (distributions shown in Fig. S5). As presented in Fig. S6, these datasets display similar patterns of O_3 diurnal changes. Since O_3 was well mixed within the ABL (Fig. S4), especially during daytime when O_3 levels are higher than those at night, the budget of ABL-mean O_3 concentration can reveal the influences of transport and photochemistry on the variations of overall O_3 levels as well as the causes of O_3 pollution in the targeted region.

Next, the contributions of various O_3-related processes in the O_3 concentration budget are discussed as follows:

- Gas-phase chemistry: Figure 4 shows that gas-phase chemistry controlled almost exclusively the O_3 concentration budget. During the morning hours, which are defined as the period from sunrise (~6:00 LT in autumn, ~5:00 LT in summer) to the O_3-peak hour (~14:00 LT), gas-phase chemistry (photochemistry) contributed to, on average, 74% and 95% of the O_3 concentration increase in autumn and summer, respectively. These contributions are notably

13

368   higher than the contributions of transport in the same periods (25% in autumn, 5% in summer). In the afternoon,

369   gas-phase chemistry was still the main process to maintain high O_3 concentrations within the PRD, but its

370   contributions gradually decreased. However, this process led to decreased O_3 concentration at night, suggesting the

371   impact of O_3 titration by emitted NO and O_3 depletion with unsaturated VOCs. It may also be related to the

372   production of particle nitrate through N_2O_5 hydrolysis (Qu et al., 2021b).

373   •   Transport: The dominance of gas-phase chemistry in the O_3 concentration budget does not mean that the influence

374   of transport on O_3 concentration can be neglected all day long. Considerable contributions of transport (mainly by

375   ABLex-H) to O_3 concentration increase are found during 2-3 hours after sunrise, with the highest hourly mean

376   contributions reaching ~40% and ~25% in autumn and summer, respectively. This result indicates the notable

377   influence of air masses with high O_3 concentrations being entrained from residual layers on near-surface O_3

378   pollution. ABLex-A and horizontal transport may contribute to the increase or decrease of ABL-mean O_3

379   concentration, depending on the O_3 levels in air parcels transported into and out of the region (further analysis is

380   provided in Sect. 3.3). Overall, these two transport processes had only limited contributions to the variations of O_3

381   concentration.

382   •   Other processes: Dry deposition contributed to a considerable decrease in O_3 concentration, especially during

383   daytime, and thus served as an important sink process for near-surface O_3. Besides, cloud process was also an

384   important sink process for O_3 in summer, which might be related to the convective vertical transport of O_3.

385

386 In summary, the results of the O_3 concentration budget indicate that gas-phase chemistry played a major role in the variations

387 of O_3 concentrations in the PRD. In particular, photochemistry led to the rapid formation of O_3 pollution during daytime,

388 rather than transport. Our conclusions agree well with those in earlier studies on the O_3 concentration budget (Lenschow et

389 al., 1981; Hou et al., 2014; Trousdell et al., 2016; Su et al., 2018; Tan et al., 2018; Tan et al., 2019; Trousdell et al., 2019; Yu

390 et al., 2020; Li et al., 2021; Yan et al., 2021).

391

392
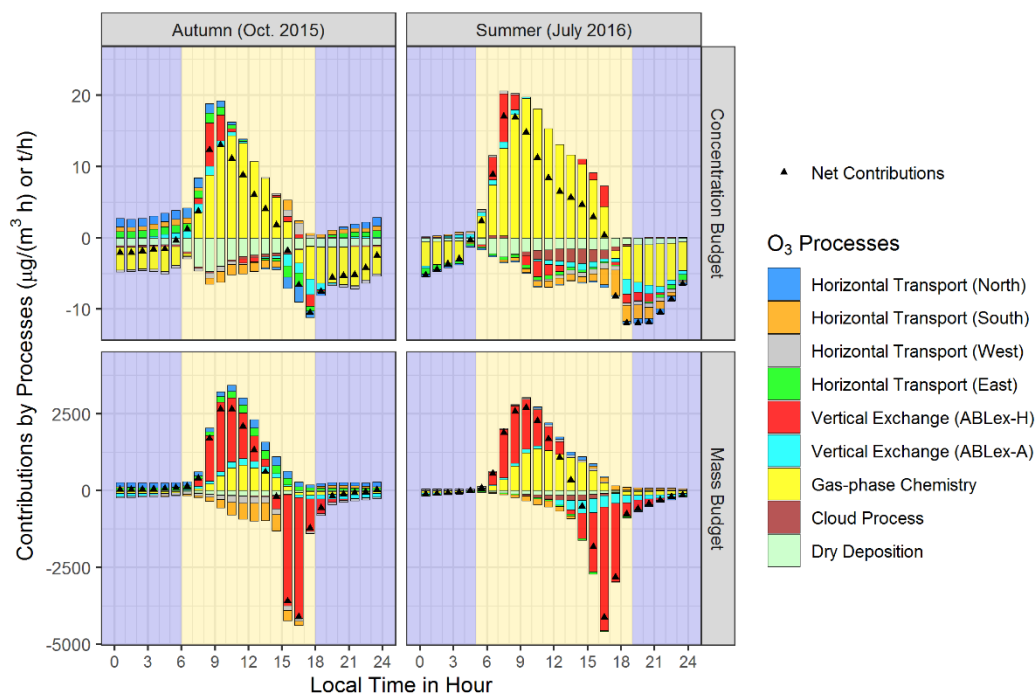
Figure 4. Mean diurnal changes of the O_3 concentration budget (upper panels) and mass budget (lower panels) on the polluted days of representative months in autumn (Oct. 2015; left panels) and summer (July 2016; right panels) within the atmospheric boundary layer of the Pearl River Delta. The units for the O_3 concentration and mass budgets are $\mu g/(m^3 \, h)$ and t/h, respectively. Backgrounds in yellow and dark blue indicate daytime and nighttime periods, respectively.

3.2 O_3 mass budget

The results of the O_3 mass budget are displayed in the lower panels of Fig. 4. The total O_3 mass within the ABL of the PRD increased during the morning hours, decreased rapidly in the afternoon and slowly at the early night, then remained stable until sunrise in both seasons. The change of total O_3 mass agrees well with the ABL diurnal cycle (Lee, 2018) — daytime ABL development (or collapse) and notable O_3 mass increase (or decrease) almost occurred simultaneously, and the negligible changes in O_3 mass during most hours of the night may be linked to the small variations of stable ABL.

We analysed the contributions of various O_3-related processes in the O_3 mass budget as well, presented as follows:

- Transport: Unlike the results of the O_3 concentration budget, transport plays a prominent role in the O_3 mass budget. On average, it contributed 78% and 53% to O_3 mass increase during the morning hours of autumn and summer, respectively, and over 90% to O_3 mass decrease during the afternoon hours of both seasons (14:00-18:00 LT in autumn and 14:00-19:00 LT in summer). Most O_3 was transported into or out of the PRD by vertical exchange through the ABL top, especially ABLex-H, which links the diurnal changes of O_3 mass and ABL. That is to say, when the height of ABL rise (drop) rapidly, a big amount of O_3 is transported into (out of) the ABL through the ABLex-H. The contributions of ABLex-A and horizontal transport to O_3 mass change were relatively limited.

15

412   However, they indicate well the characteristics and variations of regional wind fields in the PRD (more details are

413   provided in the next section).

414   •   Gas-phase chemistry: Gas-phase chemistry (photochemistry) also contributed to the increasing O_3 mass in the

415   daytime, especially in summer. However, its mean contributions during the morning hours (22% in autumn, 47% in

416   summer) were lower than those of transport.

417   •   Other processes: Dry deposition and cloud process both acted as O_3 sink processes, but with negligible

418   contributions to O_3 mass.

419

420 Based on the above discussions, transport tends to be more important than photochemistry in the O_3 mass budget, which

421 differs from the conclusions of the O_3 concentration budget. The main role of transport, especially ABLex-H, in the O_3 mass

422 budget suggests the marked impacts of the ABL diurnal cycle on regional O_3 pollution. Despite of less notable influence of

423 transport on O_3 concentration increase in comparison to that of photochemistry, massive O_3 being transported into the ABL

424 of the targeted region during the morning hours nearly determines the regional origins of O_3 pollution. Quantified results

425 combining the O_3 mass budget and source apportionment are further discussed in Sect. 4.

426 **3.3 Influences of regional wind fields on O_3 pollution: more analyses of transport contributions in O_3 budgets**

427 As discussed before, the contributions of horizontal transport and ABLex-A were relatively limited in the two O_3 budgets.

428 However, they illustrate well the influences of regional wind fields, including the seasonal prevailing winds and local

429 circulations (sea breezes), on O_3 pollution in the PRD. Two main findings from the analyses of these transport contributions

430 are presented below.

431 **3.3.1 Transport contributions in autumn: The characteristics of prevailing winds**

432 In the PRD, northerly and easterly winds prevail in autumn (as indicated by the wind roses in Fig. S3). Correspondingly, O_3

433 was transported into the PRD through its north and east borders, out of the PRD through the south and west borders, as

434 indicated by the O_3 mass budget (Fig. 4). O_3 masses transported out of the PRD were generally higher than those transported

435 into the PRD during daytime. This is attributed to higher O_3 concentrations in the downwind regions due to O_3 production

436 mostly from local emissions. "Low O_3 in, high O_3 out" also explains why horizontal transport led to the net decrease of O_3

437 concentration during daytime. At night, O_3 was still transported into the region through the north and east borders of the

438 PRD, but these processes contributed to the increase of O_3 concentrations. That is to say, with relatively higher O_3

439 concentrations compared to those in the NO_x-titrated urban atmosphere, air parcels transported from the upwind outskirts

440 served as the supply to slowdown night-time O_3 level decrease in the PRD due to chemistry and deposition.

441

442 The daytime contributions of ABLex-A in the O_3 mass budget also indicate the effects of prevailing northerly winds. The

443 PRD has mountainous regions in the northern, western and eastern outskirts, as well as urban regions with lower altitudes in

444 the central plain (Fig. S5). As shown in Fig. S7a-b, the positive contributions of ABLex-A through the ABL top (in the z-

445 direction) can be found in the mountainous northern PRD, suggesting that northerly winds resulted in the downward

446 transport of O_3 along the terrain. Daytime ABL heights in urban regions were, in general, higher than those in the

447 surrounding mountainous regions, which is the other reason why O_3 can be transported through the ABL slope (in the x-/y-

448 direction) near the urban-rural interfaces when northerly wind prevailed (Fig. S7c-d). For the O_3 concentration budget,

449 ABLex-A contributed to increased O_3 concentration during several hours after sunrise but decreased O_3 concentration in the

450 afternoon. This different effect is attributed to different comparison results between ABL and above-ABL mean O_3

451 concentrations in the two periods (O_3 concentration above the ABL is overall higher than that within the ABL in the

452 morning, while the opposite is for the afternoon; Fig. S4).

453

454 **3.3.2 Transport contributions in summer: The influence of sea breezes**

455 Although southerly winds normally prevail in summer in the PRD (Fig. S3), on O_3 polluted days, air parcels from other

456 directions could also influence the region (Qu et al., 2021a). Thus, the mean contribution of horizontal transport to O_3 mass

457 in summer was lower than in autumn. Of particular interest is the variation of the contributions of horizontal transport

458 through the south border of the PRD before and after ~14:00 LT, as indicated by the results of the O_3 mass budget (Fig. 4).

459 Besides, both O_3 budgets suggest notable O_3 mass and concentration decreases due to ABLex-A in the afternoon. These

460 phenomena are both related to the influence of sea breezes.

461

462 Figure 5 shows the near-surface wind roses at 14:00, 16:00 and 18:00 LT of O_3 polluted days in July 2016 based on the

463 observational and modelling results in the national meteorological sites within the PRD. At 14:00 LT, the main wind

464 directions were W, SW and NW in both datasets. More S and SE winds occurred in later hours, and they became the

465 prevailing winds at 18:00 LT, suggesting the gradual development of sea breezes in the PRD. Thus, O_3 was originally

466 transported out of the PRD through the south border with negative contributions to O_3 mass; in the late afternoon, sea

467 breezes reversed the directions of O_3 transport, resulting in positive contributions to O_3 mass by horizontal transport through

468 the south border (Fig. 4). Moreover, the development of sea breezes is connected to the changes of wind fields not only

469 horizontally, but also vertically. Taking the O_3 polluted day July 24th, 2016 for example, the cross-section of O_3

470 concentrations and wind fields in the PRD at 16:00 LT of the day is shown in Fig. 6 (the cross-section is made along the

471 113.2° E longitude, ranging from 26.0° to 20.0° N in latitude). Strong southerly wind and lower O_3 concentrations are found

472 in the southern PRD, indicating the influence of sea breezes during that time. Near the interfaces where sea breezes

473 encountered local air parcels (indicated by the drastic increase in O_3 concentrations from less than 100 μg/m^3 to about 100-

474 150 μg/m^3), updrafts occurred, suggesting the formation of sea breeze front (Ding et al., 2004; You and Fung, 2019). The

475 front promoted the upward transport of O_3 from the ABL, or considerable O_3 mass decrease due to ABLex-A. Both

476 horizontal transport and ABLex-A led to decreased O_3 concentrations, because under the effect of sea breezes, clean air

17

477 parcels were transported into the region and polluted air parcels were transported out of the region. The influence of sea

478 breezes can also be seen in autumn but was weaker and occurred later than in summer. Besides, in autumn, horizontal

479 transport through the south border of the PRD contributed to the increase of O_3 concentration at night, indicating the effects

480 of O_3 recirculation from the "O_3 pool" in the bay areas to the south of the PRD (Zeren et al., 2019; Zeren et al., 2022).

481

482 Through the calculations and analyses of transport contributions in the two O_3 budgets, the influences of complex transport

483 processes on multiple scales to O_3 concentration and mass can be well identified. These results provide a deeper

484 understanding of how transport influences regional O_3 pollution in the PRD.

485
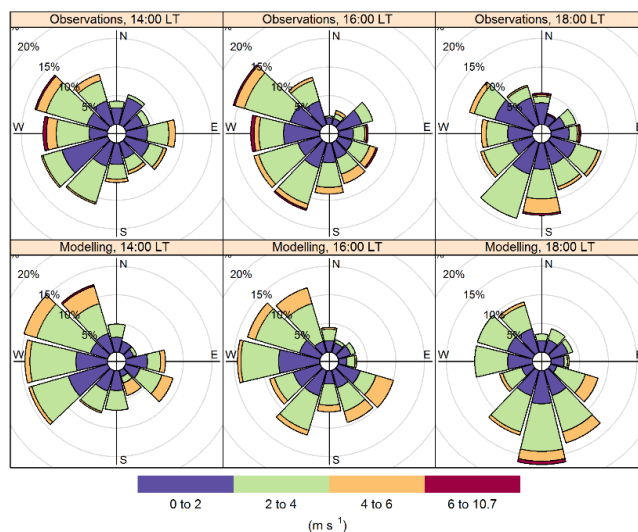
486

487 **Figure 5.** Wind roses at 14:00, 16:00, and 18:00 local time (LT) of the O_3 polluted days in July 2016 in the Pearl River Delta (PRD).
488 Observational and modelling wind speeds and directions in 29 national meteorological sites within the PRD were used for this figure.
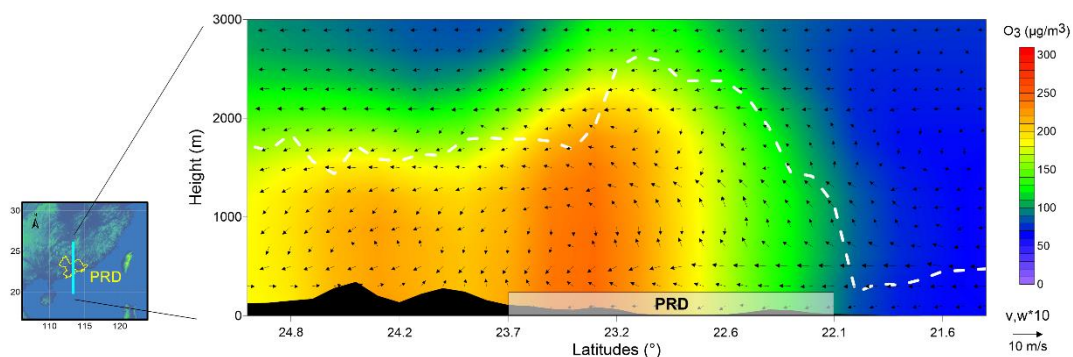
489

490 **Figure 6.** Cross-section of O_3 concentrations ($\mu g/m^3$) and wind fields at 16:00 local time on July 24th, 2016. The dashed white line
491 indicates the top of the atmospheric boundary layer. PRD, Pearl River Delta.

18

4 Effects of transport and photochemistry on the regional origins of O₃

Based on reported publications (Li et al., 2012; Li et al., 2013; Yang et al., 2019; Gao et al., 2020), O_3 in the PRD is mostly derived from emissions outside the PRD and background O_3, rather than local emissions. This is the same for the O_3 polluted days in the representative months of autumn and summer in this study, when the contributions of non-local sources account for, on average, 89% and 65% of the O_3 in the PRD, respectively, in 9:00-17:00 LT (55% and 32% contributed by BCON, 34% and 33% contributed by EC-China in the two months; Qu et al., 2021a). To explain why non-local sources are dominant for O_3 in the PRD, by combining O_3 mass budget calculation with O_3 source apportionment (method introduced in Sect. 2.6), we identified the regional origins of O_3 mass changes due to vertical exchange through the ABL top, horizontal transport and gas-phase chemistry (Fig. 7). Here, the contributions of three sources to the O_3 mass increase and decrease were both quantified. But further analyses focus on the results related to O_3 mass increase, because the origins of O_3 in the region are more likely to be influenced by the "new O_3" transported into and produced within the PRD.
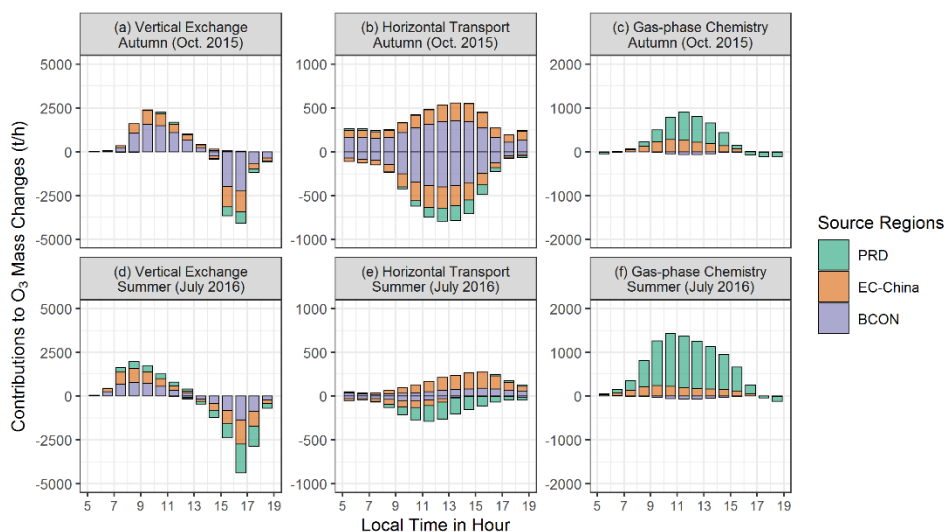
Figure 7. The regional origins of hourly O_3 mass changes contributed by (a,d) vertical exchange through the ABL top, (b,e) horizontal transport, and (c,f) gas-phase chemistry on the polluted days of representative months in autumn (Oct. 2015; a-c) and summer (July 2016; d-f). The results for the time window 5:00-19:00 LT are shown here. PRD, Pearl River Delta; EC-China, East and Central China; BCON, the boundary conditions of d02 modelling, or the contribution of sources outside the d02. Note that the scales are different among the three columns.

Through vertical exchange through the ABL top, massive non-local O_3 entered into the ABL of the PRD. In the morning-hour O_3 mass increase due to this process, BCON and EC-China accounted for 65% and 31%, respectively, in autumn. By contrast, local emissions only contributed 4% to this transported O_3 during the same period, suggesting that local O_3 was less likely to be recirculated back to the PRD during daytime. In summer, the contribution of local emissions in the O_3 mass transported into the region through vertical exchange was higher than in autumn, reaching 20% during the morning hours.

19

516   However, non-local sources still dominated the O_3 mass increase due to vertical exchange — the morning-hour contributions

517   in percentage of BCON and EC-China were 42% and 38%, respectively.

518

519   O_3 mass increase due to horizontal transport was connected to the contribution of non-local sources as well. In both seasons,

520   O_3 transported into the PRD originated almost exclusively from EC-China and BCON.

521

522   It is not surprising that most O_3 produced through photochemistry (daytime gas-phase chemistry) was related to local

523   emissions, of which the contributions accounted for 66% and 82% during the daytime of autumn (6:00-18:00 LT) and

524   summer (5:00-19:00 LT), respectively. The contributions of EC-China emissions in the daytime O_3 mass increase reached

525   34% and 18% in the two seasons, respectively, indicating that the influences of non-local O_3 precursor import on local O_3

526   photochemistry are also considerable in the PRD.

527

528   With the results of the O_3 mass budget and the regional origins of O_3 mass increase due to transport and photochemistry, the

529   effect of O_3-related processes on the origins of O_3 can be revealed. Based on the O_3 mass budget, the accumulated morning-

530   hour O_3 mass increase exceeded 10000 tons for both seasons, which is 6-9 times larger than the original O_3 mass in the ABL

531   of the PRD before sunrise (< 1500 tons). Thus, in the daytime, most O_3 in the PRD was the "new O_3" contributed by

532   transport and photochemistry, and the origins of O_3 within the region were nearly determined by these of newly transported

533   and produced O_3. By combining the O_3 mass budget and O_3 source apportionment, we identified the O_3 mass increase due to

534   O_3-related processes as local (PRD) and non-local (EC-China and BCON) contributions. According to the results discussed

535   before, high contributions of transport in the morning-hour O_3 mass increase and the dominance of non-local source

536   contributions in this part of new O_3 ensure that non-local sources contributed to most O_3 in the PRD. Moreover, differences

537   in the contributions of O_3-related processes in the O_3 mass budget as well as the origins of morning-hour O_3 mass increase

538   lead to varied origins of O_3 in the region. For instance, when comparing the results of O_3 source apportionment in the two

539   seasons, we found that the contributions of non-local sources (local emissions) to O_3 were lower (higher) in summer than in

540   autumn. It can be attributed to the combined effects of increased photochemistry contributions (or decreased transport

541   contributions) in the O_3 mass increase and reduced non-local source contributions in both transported and chemically

542   produced O_3 in summer. Collectively, these changes lead to reduced non-local contributions (or higher local contributions) to

543   O_3.

544

545   By influencing O_3 mass increase and its regional origins, transport and photochemistry determine the results of O_3 source

546   apportionment within the region. Specifically, transport (mainly ABLex-H) brings massive non-local O_3 into the region in

547   the morning, explaining why most O_3 in the PRD is derived from non-local sources. However, accompanied with the

548   simultaneous rapid increase of ABL volumes, this process has a relatively limited contribution to O_3 concentration increase

549   in comparison to photochemistry. The O_3 concentration budget only concerns the influence of O_3-related processes on the

550 variations of O_3 concentration, thus it fails to illustrate the effect of transport on the regional origin of O_3. Our results

551 highlight the difference between the O_3 concentration and mass budgets, which may result in distinct understandings about

552 the role of transport and photochemistry in regional O_3 pollution. To completely illustrate the effects of two O_3-related

553 processes on regional O_3 pollution, insights from both O_3 budgets are required.

5 Conclusion and outlook

555 To effectively alleviate O_3 pollution, it is important to understand the respective role of transport and photochemistry in

556 regional O_3 pollution. The O_3 concentration budget is widely used to quantify the contributions of these O_3-related processes

557 to the variations of O_3 concentrations, and it often concludes that photochemistry is the main contributor to the aggravation

558 of O_3 pollution. However, it does not explain why most of the O_3 is transported from the outside regions as indicated by O_3

559 source apportionment studies. To comprehensively illustrate the effects of transport and photochemistry on regional O_3

560 pollution, based on the modelling results of WRF-CMAQ, this study presents a method to quantify not only the O_3

561 concentration budget, but also the O_3 mass budget, in which the contributions of O_3-related processes (including transport

562 and photochemistry) to the variations of mean O_3 concentrations and total O_3 mass within the ABL of the PRD are separately

563 identified. The different effects of transport on O_3 concentration and mass were considered in the above calculations. The O_3

564 concentration budget in the PRD reveals that gas-phase chemistry, including daytime photochemistry and night-time O_3

565 titration/depletion, drives the variations of O_3 concentration. Particularly, photochemistry contributed 74% and 95% to the

566 O_3 concentration increase in the morning hours of autumn and summer months, respectively. In contrast, transport,

567 especially the vertical exchange through the ABL top, is the main process contributing to the O_3 mass increase in the

568 morning (78% and 53% in autumn and summer, respectively) and decrease in the afternoon (> 90%). The diurnal changes of

569 transport contributions in the two O_3 budgets are closely connected to the variations of the ABL and regional wind fields,

570 including the seasonal prevailing winds and local circulations (sea breezes), in the PRD. Massive O_3, mostly derived from

571 non-local sources, being transported into the ABL in the morning has a relatively limited influence on the O_3 concentration

572 increase (25% and 5% in autumn and summer, respectively) compared to photochemistry because of the rapid change of

573 ABL volumes at the same time. However, this process nearly determines the dominance of non-local source contributions

574 for daytime O_3 in the PRD. The two O_3 budgets show notable differences, but together they provide a more complete

575 overview of the effects of transport and photochemistry on regional O_3 pollution.

576

577 It should be noted that the conclusions in this study apply not only to O_3, but also to other pollutants with moderately long

578 atmospheric lifetimes, including fine particulate matter and some of its components. In theory, transport and chemical

579 transformations are both important processes for these pollutants. However, transport has different effects on the

580 concentration and mass of pollutants on an hourly scale, which is similar to the discussion in Sect. 2.4. Furthermore, besides

581 regional origins, the difference between the two budgets may also contribute to the inconsistency of other characteristics of

582   pollutants, such as the contributions of different reaction pathways and sensitivities to precursor emissions, identified by the

583   concentration budget and mass-based methods. When large quantities of pollutants with different characteristics are

584   transported into the region, the variation of their concentrations is often not perceptible and thus neglected in the

585   concentration budget. However, as indicated by this study, the transport processes are likely to change or even determine the

586   characteristics of pollutants within the region. Therefore, we suggest that attention should be paid to selecting a proper

587   budget type and using correct budget calculation methods in related research. But to fully reveal the effects of transport,

588   chemistry and other related processes on regional pollution, insights from both concentration and mass budgets are

589   necessary.

590

591   Uncertainty remains in the calculated O_3 budgets, which is partly related to the biases in the modelling results. Therefore,

592   supporting observations are essential for future research. Recent progress in observational techniques (Zhao et al., 2021;

593   Zhou et al., 2021) has enabled three-dimensional measurements of meteorological parameters and O_3 concentrations with

594   high spatiotemporal resolution and coverage. These data can be used not only for the model validation of key parameters in

595   budget calculations, but also for the comparisons between observation- and modelling-based contributions by various O_3-

596   related processes in O_3 budgets (Kaser et al., 2017). The comparison of contributions by O_3-related processes is indicative of

597   the main uncertainties in O_3 pollution modelling, and is therefore also important for further model developments.

598

599   The present study concluded that transport and gas-phase chemistry play the main role in the O_3 mass and concentration

600   budgets, respectively. As a consequence of our assessment, the following is suggested for policy-makers. For areas where

601   non-local emissions notably contribute to O_3, emission reduction in the upwind regions can reduce the overall O_3

602   concentrations effectively, which is a crucial step towards the long-term improvement of regional air quality. However, for

603   short-term air pollution control, this strategy is not efficient because emission reduction in upwind regions may need to start

604   days earlier before the polluted periods. In contrast, reducing local emissions is expected to lower the rapid daytime O_3

605   concentration increase efficiently and, thereby, O_3 peak levels in the short term, as highlighted by the O_3 concentration

606   budget. The choice of the better strategy to be applied should depend on the specific objectives of O_3 control (mean levels vs.

607   peak levels; long-term vs. short-term), which are set based on a more in-depth understanding of O_3 effects on human health,

608   crop yields and ecosystems. More efforts are required to systematically evaluate the effects of different emission reduction

609   strategies on alleviating the detrimental effects of O_3.

610

611   *Data availability.* The source codes of WRF and CMAQ are available at the site

612   https://www2.mmm.ucar.edu/wrf/users/download/get_sources.html and https://www.cmascenter.org/cmaq/, respectively.

613   FNL meteorological input files were downloaded from the site https://rda.ucar.edu/datasets/ds083.2/. MEIC v1.3

614   anthropogenic emission inventory is available at http://meicmodel.org/?page_id=560. The source codes of MEGAN can be

615   found at https://bai.ess.uci.edu/megan/data-and-code. IAGOS dataset used in model validation was searched and downloaded

616 from http://iagos-data.fr, which includes all profiles measured in flights taking off from and landing in Hong Kong during

617 the two representative months. We also provided the initial Fortran code used in ozone budget calculations and hourly O_3

618 concentration and mass budget results in the two representative months (the initial data of Fig. 4) at

619 https://doi.org/10.5281/zenodo.6259253.

620

621 *Author contributions.* KQ, XW and YZ designed the study. KQ, XW, TX did the simulations using the WRF-CMAQ model.

622 JS, LZ and YZ provided observational results for model validation. KQ, XW, XC, YY, XJ and YZ developed the post-

623 processing tool *flux_4d_cal*, conducted and analysed O_3 budget results. KQ, XW, MV, MK, GB and YZ wrote and/or revised

624 this paper, with critical feedbacks from all other authors.

625

626 *Competing interests.* One of the authors is a member of the editorial board of Atmospheric Chemistry and Physics, and the

627 peer-review process was guided by an independent editor. The authors declare no other conflict of interest.

628

632

References

Ainsworth, E. A.: Understanding and improving global crop response to ozone pollution, Plant J., 90, 886–897, https://doi.org/10.1111/tpj.13298, 2017.

Bates, K. H. and Jacob, D. J.: An expanded definition of the odd oxygen family for tropospheric ozone budgets: Implications for ozone lifetime and stratospheric influence, Geophys. Res. Lett., 47, e2019GL084486, https://doi.org/10.1029/2019GL084486, 2019.

Boian, C. and Andrade, M. D. F.: Characterization of ozone transport among metropolitan regions, Rev. Bras. Meteorol., 27, 229-242, https://doi.org/10.1590/S0102-77862012000200009, 2012.

Carter, W. P. L.: Development of the SAPRC-07 chemical mechanism, Atmos. Environ., 44, 5324–5335, https://doi.org/10.1016/j.atmosenv.2010.01.026, 2010.

Chang, X., Wang, S., Zhao, B., Cai, S., and Hao, J.: Assessment of inter-city transport of particulate matter in the Beijing–Tianjin–Hebei region, Atmos. Chem. Phys., 18, 4843–4858, https://doi.org/10.5194/acp-18-4843-2018, 2018.

Clappier, A., Belis, C. A., Pernigotti, D., and Thunis, P.: Source apportionment and sensitivity analysis: two methodologies with two different purposes, Geosci. Model Dev., 10, 4245–4256, https://doi.org/10.5194/gmd-10-4245-2017, 2017.

Ding, A., Wang, T., Zhao, M., Wang, T. J., and Li, Z. K.: Simulation of sea-land breezes and a discussion of their implications on the transport of air pollution during a multi-day ozone episode in the Pearl River Delta of China, Atmos. Environ., 38, 6737–6750, https://doi.org/10.1016/j.atmosenv.2004.09.017, 2004.

Fishman, J., Wozniak, A. E., and Creilson, J. K.: Global distribution of tropospheric ozone from satellite measurements using the empirically corrected tropospheric ozone residual technique: Identification of the regional aspects of air pollution, Atmos. Chem. Phys., 3, 893–907, https://doi.org/10.5194/acp-3-893-2003, 2003.

Fleming, Z. L., Doherty, R. M., von Schneidemesser, E., Malley, C. S., Cooper, O. R., Pinto, J. P., Colette, A., Xu, X. B., Simpson, D., Schultz, M. G., Lefohn, A. S., Hamad, S., Moolla, R., Solberg, S., and Feng, Z. Z.: Tropospheric ozone assessment report: Present-day ozone distribution and trends relevant to human health, Elementa-Sci. Anthrop., 6, 12, https://doi.org/10.1525/elementa.273, 2018.

Fowler, D., Brimblecombe, P., Burrows, J., Heal, M. R., Grennfelt, P., Stevenson, D. S., Jowett, A., Nemitz, E., Coyle, M., Liu, X., Chang, Y., Fuller, G. W., Sutton, M. A., Klimont, Z., Unsworth, M. H., and Vieno, M.: A chronology of global air quality, Philos. T. R. Soc. A, 378, 20190314, https://doi.org/10.1098/rsta.2019.0314, 2020.

Gao, M., Gao, J., Zhu, B., Kumar, R., Lu, X., Song, S., Zhang, Y., Jia, B., Wang, P., Beig, G., Hu, J., Ying, Q., Zhang, H., Sherman, P., and McElroy, M. B.: Ozone pollution over China and India: seasonality and sources, Atmos. Chem. Phys., 20, 4399–4414, https://doi.org/10.5194/acp-20-4399-2020, 2020.

Gao, X., Deng, X., Tan, H., Wang, C., Wang, N., and Yue, D.: Characteristics and analysis on regional pollution process and circulation weather types over Guangdong Province, Acta Scientiae Circumstantiae (in Chinese), 38(5), 1708–1716, https://doi.org/10.13671/j.hjkxxb.2017.0473, 2018.

666 Guo, J. J., Fiore, A. M., Murray, L. T., Jaffe, D. A., Schnell, J. L., Moore, C. T., and Milly, G. P.: Average versus high

667   surface ozone levels over the continental USA: model bias, background influences, and interannual variability, Atmos.

668   Chem. Phys., 18, 12123–12140, https://doi.org/10.5194/acp-18-12123-2018, 2018.

669 He, K.: Multi-resolution Emission Inventory for China (MEIC): model framework and 1990-2010 anthropogenic emissions,

670   American Geophysical Union, Fall Meeting 2012, 3–7 December 2012, San Francisco, USA, A32B-05, 2012.

671 Hou, X., Zhu, B., Kang, H., and Gao, J.: Analysis of seasonal ozone budget and spring ozone latitudinal gradient variation in

672   the boundary layer of the Asia-Pacific region, Atmos. Environ., 94, 734–741,

673   https://doi.org/10.1016/j.atmosenv.2014.06.006, 2014.

674 Hu, J., Li, Y., Zhao, T., Liu, J., Hu, X.-M., Liu, D., Jiang, Y., Xu, J., and Chang, L.: An important mechanism of regional O_3

675   transport for summer smog over the Yangtze River Delta in eastern China, Atmos. Chem. Phys., 18, 16239–16251,

676   https://doi.org/10.5194/acp-18-16239-2018, 2018.

677 Janssen, R. H. H. and Pozzer, A.: Description and implementation of a MiXed Layer model (MXL, v1.0) for the dynamics of

678   the atmospheric boundary layer in the Modular Earth Submodel System (MESSy), Geosci. Model Dev., 8, 453–471,

679   https://doi.org/10.5194/gmd-8-453-2015, 2015.

680 Jin, X., Cai, X., Huang, Q., Wang, X., Song, Y., and Zhu, T.: Atmospheric boundary layer—free troposphere air exchange in

681   the North China Plain and its impact on $PM_{2.5}$ pollution, J. Geophys. Res.-Atmos., 126(9), e2021JD034641,

682   https://doi.org/10.1029/2021JD034641, 2021.

683 Kaser, L., Patton, E. G., Pfister, G. G., Weinheimer, A. J., Montzka, D. D., Flocke, F., Thompson, A. M., Stauffer, R. M.,

684   and Halliday, H. S.: The effect of entrainment through atmospheric boundary layer growth on observed and modeled

685   surface ozone in the Colorado Front Range, J. Geophys. Res.-Atmos., 122, 6075–6093,

686   https://doi.org/10.1002/2016JD026245, 2017.

687 Laughner, J. L. and Cohen, R. C.: Direct observation of changing NOx lifetime in North American cities, Science, 366, 723–

688   727, https://doi.org/10.1126/science.aax6832, 2019.

689 Lee, X.: Fundamentals of Boundary-Layer Meteorology, Springer Atmospheric Sciences., 2018.

690 Lelieveld, J., Hoor, P., Jöckel, P., Pozzer, A., Hadjinicolaou, P., Cammas, J.-P., and Beirle, S.: Severe ozone air pollution in

691   the Persian Gulf region, Atmos. Chem. Phys., 9, 1393–1406, https://doi.org/10.5194/acp-9-1393-2009, 2009.

692 Lenschow, D. H., Pearson, R., and Stankov, B. B.: Estimating the ozone budget in the boundary layer by use of aircraft

693   measurements of ozone eddy flux and mean concentration, J. Geophys. Res., 86, 7291–7297,

694   https://doi.org/10.1029/JC086iC08p07291, 1981.

695 Li, L., Xie, F., Li, J., Gong, K., Xie, X., Qin, Y., Qin, M., and Hu, J.: Diagnostic analysis of regional ozone pollution in

696   Yangtze River Delta, China: A case study in summer 2020, Sci. Total Environ., 812, 151511,

697   https://doi.org/10.1016/j.scitotenv.2021.151511, 2021.

698 Li, M., Zhang, Q., Kurokawa, J.-I., Woo, J.-H., He, K., Lu, Z., Ohara, T., Song, Y., Streets, D. G., Carmichael, G. R., Cheng,

699   Y., Hong, C., Huo, H., Jiang, X., Kang, S., Liu, F., Su, H., and Zheng, B.: MIX: a mosaic Asian anthropogenic emission

700   inventory under the international collaboration framework of the MICS-Asia and HTAP, Atmos. Chem. Phys., 17, 935–

701   963, https://doi.org/10.5194/acp-17-935-2017, 2017.

702   Li, Y., Lau, A. K. H., Fung, J. C. H., Ma, H., and Tse, Y.: Systematic evaluation of ozone control policies using an Ozone

703   Source Apportionment method, Atmos. Environ., 76, 136–146, https://doi.org/10.1016/j.atmosenv.2013.02.033, 2013.

704   Li, Y., Lau, A. K. H., Fung, J. C. H., Zheng, J.Y., Zhong, L. J., and Louie, P. K. K.: Ozone source apportionment (OSAT) to

705   differentiate local regional and super-regional source contributions in the Pearl River Delta region, China, J. Geophys.

706   Res.-Atmos., 117, D15305, http://doi.org/10.1029/2011JD017340, 2012.

707   Liu, F., Beirle, S., Zhang, Q., Dörner, S., He, K., and Wagner, T.: NOx lifetimes and emissions of cities and power plants in

708   polluted background estimated by satellite observations, Atmos. Chem. Phys., 16, 5283–5298,

709   https://doi.org/10.5194/acp-16-5283-2016, 2016.

710   Liu, H. L., Zhang, M. G., and Han, X.: A review of surface ozone source apportionment in China, Atmos. Ocean. Sci. Lett.,

711   13, 470–484, https://doi.org/10.1080/16742834.2020.1768025, 2020.

712   Liu, P., Zhang, Y., Yu, S. C., and Schere, K. L.: Use of a Process Analysis tool for diagnostic study on fine particulate matter

713   predictions in the U.S. Part II: Process Analysis and sensitivity simulations, Atmos. Pollut. Res., 2, 61–71,

714   https://doi.org/10.5094/APR.2011.008, 2011.

715   Massagué, J., Carnerero, C., Escudero, M., Baldasano, J. M., Alastuey, A., and Querol, X.: 2005–2017 ozone trends and

716   potential benefits of local measures as deduced from air quality measurements in the north of the Barcelona

717   metropolitan area, Atmos. Chem. Phys., 19, 7445–7465, https://doi.org/10.5194/acp-19-7445-2019, 2019.

718   Mills, G., Wagg, S., and Harmens, H.: Ozone pollution: impacts on ecosystem services and biodiversity (CEH Project no.

719   C04062, C04325), Bangor, UK, NERC/Centre for Ecology & Hydrology, 2013.

720   Myriokefalitakis, S., Daskalakis, N., Fanourgakis, G. S., Voulgarakis, A., Krol, M. C., de Brugh, J. A., and Kanakidou, M.:

721   Ozone and carbon monoxide budgets over the Eastern Mediterranean, Sci. Total Environ., 563, 40-52,

722   https://doi.org/10.1016/j.scitotenv.2016.04.061, 2016.

723   Naik, V., Szopa, S., Adhikary, B., Artaxo, P., Berntsen, T., Collins, W. D., Fuzzi, S., Gallardo, L., Kiendler Scharr, A.,

724   Klimont, Z., Liao, H., Unger, N., and Zanis, P.: Short-Lived Climate Forcers, in: Climate Change 2021: The Physical

725   Science Basis. Contribution of Working Group I to the Sixth Assessment Report of the Intergovernmental Panel on

726   Climate Change, edited by: Masson-Delmotte, V., Zhai, P., Pirani, A., Connors, S. L., Péan, C., Berger, S., Caud, N.,

727   Chen, Y., Goldfarb, L., Gomis, M. I., Huang, M., Leitzell, K., Lonnoy, E., Matthews, J. B. R., Maycock, T. K.,

728   Waterfield, T., Yelekçi, O., Yu, R., and Zhou, B., Cambridge University Press, Cambridge, United Kingdom and New

729   York, NY, USA, 817–922, https://doi.org/10.1017/9781009157896.008, 2021.

730   Novel, D. P.: The OTC challenge: Adding VOC controls in the northeast, J. Air Waste Manag. Assoc., 42(8), 1053-1056,

731   https://doi.org/10.1080/10473289.1992.10467050, 1992.

Pay, M. T., Gangoiti, G., Guevara, M., Napelenok, S., Querol, X., Jorba, O., and Pérez García-Pando, C.: Ozone source apportionment during peak summer events over southwestern Europe, Atmos. Chem. Phys., 19, 5467–5494, https://doi.org/10.5194/acp-19-5467-2019, 2019.

Petzold, A., Thouret, V., Gerbig, C., Zahn, A., Brenninkmeijer, C. A. M., Gallagher, M., Hermann, M., Pontaud, M., Ziereis, H., Boulanger, D., Marshall, J., Nédélec, P., Smit, H. G. J., Friess, U., Flaud, J.-M., Wahner, A., Cammas, J.-P., Volz-Thomas, A. and IAGOS TEAM: Global-scale atmosphere monitoring by in-service aircraft–current achievements and future prospects of the European Research Infrastructure IAGOS, Tellus B, 67, 28452, https://doi.org/10.3402/tellusb.v67.28452, 2015.

Qu, K., Wang, X., Xiao, T., Shen, J., Lin, T., Chen, D., He, L., Huang, X., Zeng, L., Lu, K., Ou, Y., and Zhang, Y.: Cross-regional transport of $PM_{2.5}$ nitrate in the Pearl River Delta, China: Contributions and mechanisms, Sci. Total Environ., 753, 142439, https://doi.org/10.1016/j.scitotenv.2020.142439, 2021b.

Qu, K., Wang, X., Yan, Y., Shen, J., Xiao, T., Dong, H., Zeng, L., and Zhang, Y.: A comparative study to reveal the influence of typhoons on the transport, production and accumulation of O_3 in the Pearl River Delta, China, Atmos. Chem. Phys., 21, 11593–11612, https://doi.org/10.5194/acp-21-11593-2021, 2021a.

Reid, N., Yap, D., and Bloxam, R.: The potential role of background ozone on current and emerging air issues: An overview, Air Qual. Atmos. Health, 1, 19–29, https://doi.org/10.1007/s11869-008-0005-z, 2008.

Schultz, M. G., Schröder, S., Lyapina, O., Cooper, O., Galbally, I., Petropavlovskikh, I., Von Schneidemesser, E., Tanimoto, H., Elshorbany, Y., Naja, M., Seguel, R., Dauert, U., Eckhardt, P., Feigenspahn, S., Fiebig, M., Hjellbrekke, A.-G., Hong, Y.-D., Kjeld, P. C., Koide, H., Lear, G., Tarasick, D., Ueno, M., Wallasch, M., Baumgardner, D., Chuang, M.-T., Gillett, R., Lee, M., Molloy, S., Moolla, R., Wang, T., Sharps, K., Adame, J. A., Ancellet, G., Apadula, F., Artaxo, P., Barlasina, M., Bogucka, M., Bonasoni, P., Chang, L., Colomb, A., Cuevas, E., Cupeiro, M., Degorska, A., Ding, A., Fröhlich, M., Frolova, M., Gadhavi, H., Gheusi, F., Gilge, S., Gonzalez, M. Y., Gros, V., Hamad, S. H., Helmig, D., Henriques, D., Hermansen, O., Holla, R., Huber, J., Im, U., Jaffe, D. A., Komala, N., Kubistin, D., Lam, K.-S., Laurila, T., Lee, H., Levy, I., Mazzoleni, C., Mazzoleni, L., McClure-Begley, A., Mohamad, M., Murovic, M., Navarro-Comas, M., Nicodim, F., Parrish, D., Read, K. A., Reid, N., Ries, L., Saxena, P., Schwab, J. J., Scorgie, Y., Senik, I., Simmonds, P., Sinha, V., Skorokhod, A., Spain, G., Spangl, W., Spoor, R., Springston, S. R., Steer, K., Steinbacher, M., Suharguniyawan, E., Torre, P., Trickl, T., Weili, L., Weller, R., Xu, X., Xue, L., and Zhiqiang, M.: Tropospheric ozone assessment report: Database and metrics data of global surface ozone observations, Elementa-Sci. Anthrop., 5, 58, https://doi.org/10.1525/elementa.244, 2017.

Seinfeld, J. H. and Pandis, S. N.: Atmospheric chemistry and physics: from air pollution to climate change, John Wiley & Sons, 2016.

Sinclair, V. A., Belcher, S. E., and Gray, S. L.: Synoptic controls on boundary-layer characteristics, Bound.-Layer Meteorol., 134, 387–409, https://doi.org/10.1007/s10546-009-9455-6, 2010.

765 Sitch, S., Cox, P. M., Collins, W. J., and Huntingford, C.: Indirect radiative forcing of climate change through ozone effects

766   on the land-carbon sink, Nature, 448, 791–795, https://doi.org/10.1038/nature06059, 2007.

767 Stevenson, D. S., Dentener, F. J., Schultz, M. G., Ellingsen, K., van Noije, T. P. C., Wild, O., Zeng, G., Amann, M.,

768   Atherton, C. S., Bell, N., Bergmann, D. J., Bey, I., Butler, T., Cofala, J., Collins, W. J., Derwent, R. G., Doherty, R. M.,

769   Drevet, J., Eskes, H. J., Fiore, A. M., Gauss, M., Hauglustaine, D. A., Horowitz, L. W., Isaksen, I. S. A., Krol, M. C.,

770   Lamarque, J.-F., Lawrence, M. G., Montanaro, V., Müller, J.-F., Pitari, G., Prather, M. J., Pyle, J. A., Rast, S.,

771   Rodriguez, J. M., Sanderson, M. G., Savage, N. H., Shindell, D. T., Strahan, S. E., Sudo, K., and Szopa, S.: Multimodel

772   ensemble simulations of present-day and near-future tropospheric ozone, J. Geophys. Res., 111, D08301,

773   https://doi.org/10.1029/2005JD006338, 2006.

774 Su, R., Lu, K. D., Yu, J. Y., Tan, Z. F., Jiang, M. Q., Li, J., Xie, S. D., Wu, Y. S., Zeng, L. M., Zhai, C. Z., and Zhang, Y. H.:

775   Exploration of the formation mechanism and source attribution of ambient ozone in Chongqing with an observation-

776   based model, Sci. China Earth Sci., 61, 23–32, https://doi.org/10.1007/s11430-017-9104-9, 2018.

777 Tan, Z., Lu, K., Jiang, M., Su, R., Dong, H., Zeng, L., Xie, S., Tan, Q., and Zhang, Y.: Exploring ozone pollution in

778   Chengdu, southwestern China: A case study from radical chemistry to O_3-VOC-NO_x sensitivity, Sci. Total Environ.,

779   636, 775–786, https://doi.org/10.1016/j.scitotenv.2018.04.286, 2018.

780 Tan, Z., Lu, K., Jiang, M., Su, R., Wang, H., Lou, S., Fu, Q., Zhai, C., Tan, Q., Yue, D., Chen, D., Wang, Z., Xie, S., Zeng,

781   L., and Zhang, Y.: Daytime atmospheric oxidation capacity in four Chinese megacities during the photochemically

782   polluted season: a case study based on box model simulation, Atmos. Chem. Phys., 19, 3493–3513,

783   https://doi.org/10.5194/acp-19-3493-2019, 2019.

784 Thunis, P., Clappier, A., Tarrason, L., Cuvelier, C., Monteiro, A., Pisoni, E., Wesseling, J., Belis, C. A., Pirovano, G.,

785   Janssen, S., Guerreiro, C., and Peduzzi, E.: Source apportionment to support air quality planning: Strengths and

786   weaknesses of existing approaches, Environ. Int., 130, 104825, https://doi.org/10.1016/j.envint.2019.05.019, 2019.

787 Trousdell, J. F., Caputi, D., Smoot, J., Conley, S. A., and Faloona, I. C.: Photochemical production of ozone and emissions

788   of NO_x and CH_4 in the San Joaquin Valley, Atmos. Chem. Phys., 19, 10697–10716, https://doi.org/10.5194/acp-19-

789   10697-2019, 2019.

790 Trousdell, J. F., Conley, S. A., Post, A., and Faloona, I. C.: Observing entrainment mixing, photochemical ozone production,

791   and regional methane emissions by aircraft using a simple mixed-layer framework, Atmos. Chem. Phys., 16, 15433–

792   15450, https://doi.org/10.5194/acp-16-15433-2016, 2016.

793 Vilà-Guerau De Arellano, J., van Heerwaarden, C. C., van Stratum, B. J. H., and van den Dries, K.: Atmospheric Boundary

794   Layer: Integrating Air Chemistry and Land Interactions, Cambridge University Press, New York, 2015.

795 Yan, F., Gao, Y., Ma, M., Liu, C., Ji, X., Zhao, F., Yao, X., and Gao, H.: Revealing the modulation of boundary conditions

796   and governing processes on ozone formation over northern China in June 2017, Environ. Pollut., 272, 115999,

797   https://doi.org/10.1016/j.envpol.2020.115999, 2021.

798   Yang, L., Wang, X., and Chen, Q.: New method for investigating regional interactions of air pollutants (in Chinese), Acta
799   Sci. Circumstantiae, 32(3), 528-536, https://doi.org/10.13671/j.hjkxxb.2012.03.012, 2012.

800   Yang, W., Chen, H., Wang, W., Wu, J., Li, J., Wang, Z., Zheng, J., and Chen, D.: Modeling study of ozone source
801   apportionment over the Pearl River Delta in 2015, Environ. Pollut., 253, 393-402,
802   https://doi.org/10.1016/j.envpol.2019.06.091, 2019.

803   You, C., and Fung, J. C. H.: Characteristics of the sea-breeze circulation in the Pearl River Delta region and its dynamical
804   diagnosis. Journal of Applied Meteorology and Climatology, 58(4), 741-755, https://doi.org/10.1175/JAMC-D-18-
805   0153.1, 2019.

806   Yu, D., Tan, Z., Lu, K., Ma, X., Li, X., Chen, S., Zhu, B., Lin, L., Li, Y., Qiu, P., Yang, X., Liu, Y., Wang, H., He, L.,
807   Huang, X., and Zhang, Y.: An explicit study of local ozone budget and NO_x-VOCs sensitivity in Shenzhen China,
808   Atmos. Environ., 224, 117304, https://doi.org/10.1016/j.atmosenv.2020.117304, 2020.

809   Zeren, Y., Guo, H., Lyu, X., Jiang, F., Wang, Y., Liu, X., Zeng, L., Li, M., and Li, L.: An Ozone "Pool" in South China:
810   Investigations on Atmospheric Dynamics and Photochemical Processes Over the Pearl River Estuary, J. Geophys. Res.,
811   124, 12340–12355, https://doi.org/10.1029/2019jd030833, 2019.

812   Zeren, Y., Zhou, B., Zheng, Y., Jiang, F., Lyu, X., Xue, L., Wang, H., Liu, X., and Guo, H.: Does Ozone Pollution Share the
813   Same Formation Mechanisms in the Bay Areas of China?, Environ. Sci. Tech., 56(20), 14326-14337,
814   https://doi.org/10.1021/acs.est.2c05126, 2022.

815   Zhang, J. J., Wei, Y., and Fang, Z.: Ozone pollution: A major health hazard worldwide, Front. Immunol., 10, 2518,
816   https://doi.org/10.3389/fimmu.2019.02518, 2019.

817   Zhao, R., Hu, Q., Sun, Z., Wu, Y., Xing, C., Liu, H., and Liu, C.: Review of space and ground integrated remote sensing for
818   air pollutants (in Chinese). Res. Environ. Sci., 34(1), 28-40. https://doi.org/10.13198/j.issn.1001-6929.2020.11.25,
819   2021.

820   Zhao, W., Tang, G., Yu, H., Yang, Y., Wang, Y., Wang, L., An, J., Gao, W., Hu, B., Cheng, M., An, X., Li, X., and Wang,
821   Y.: Evolution of boundary layer ozone in Shijiazhuang, a suburban site on the North China Plain, J. Environ. Sci., 83,
822   152–160, https://doi.org/10.1016/j.jes.2019.02.016, 2019.

823   Zhou, B., Zhang, S., Xue, R., Li, J., and Wang, S.: A review of Space-Air-Ground integrated remote sensing techniques for
824   atmospheric monitoring, J. Environ. Sci., https://doi.org/10.1016/j.jes.2021.12.008, 2021.

825